GEOLOGY | THE GEOLOGICAL SOCIETY OF AMERICA®

https://doi.org/10.1130/G47223.1

Manuscript received 18 November 2019
Revised manuscript received 1 March 2020
Manuscript accepted 3 March 2020

© 2020 Geological Society of America. For permission to copy, contact editing@geosociety.org.

Stacked sills forming a deep melt-mush feeder conduit beneath Axial Seamount

Suzanne M. Carbotte[1], Adrien Arnulf[2], Marc Spiegelman[1], Michelle Lee[1], Alistair Harding[3], Graham Kent[4], Juan Pablo Canales[5] and Mladen Nedimović[6]

[1]Lamont-Doherty Earth Observatory, Columbia University, Palisades, New York 10964, USA
[2]Institute for Geophysics, University of Texas at Austin, Austin, Texas 78758, USA
[3]Scripps Institution of Oceanography, University of California–San Diego, La Jolla, California 92037, USA
[4]Nevada Seismological Laboratory, University of Nevada–Reno, Reno, Nevada 89557, USA
[5]Department of Geology and Geophysics, Woods Hole Oceanographic Institution, Woods Hole, Massachusetts 02543, USA
[6]Department of Earth Sciences, Dalhousie University, Halifax, Nova Scotia B3H 4R2, Canada

ABSTRACT

Magmatic systems are composed of melt accumulations and crystal mush that evolve with melt transport, contributing to igneous processes, volcano dynamics, and eruption triggering. Geophysical studies of active volcanoes have revealed details of shallow-level melt reservoirs, but little is known about fine-scale melt distribution at deeper levels dominated by crystal mush. Here, we present new seismic reflection images from Axial Seamount, northeastern Pacific Ocean, revealing a 3–5-km-wide conduit of vertically stacked melt lenses, with near-regular spacing of 300–450 m extending into the inferred mush zone of the mid-to-lower crust. This column of lenses underlies the shallowest melt-rich portion of the upper-crustal magma reservoir, where three dike intrusion and eruption events initiated. The pipe-like zone is similar in geometry and depth extent to the volcano inflation source modeled from geodetic records, and we infer that melt ascent by porous flow focused within the melt lens conduit led to the inflation-triggered eruptions. The multiple near-horizontal lenses are interpreted as melt-rich layers formed via mush compaction, an interpretation supported by one-dimensional numerical models of porous flow in a viscoelastic matrix.

INTRODUCTION

There is growing recognition of the importance of crystal mush zones for igneous processes in volcanic systems (e.g., Cashman et al., 2017). Recent syntheses of diverse observations from volcanic arc and intraplate volcanoes as well as physical models of igneous processes challenge the classic model of long-lived, large, melt-rich shallow reservoirs and have led to an emerging view of magmatic systems as transcrustal and mush-dominated systems (e.g., Annen et al., 2005; Cashman et al., 2017; Sparks et al., 2019). In submarine volcanic systems, this view has been supported by geophysical studies of mid-ocean ridges dating back to the late 1980s, which revealed a volumetrically dominant crystal mush zone in the mid-to-lower oceanic crust beneath a shallow upper-crustal magma body (Sinton and Detrick, 1992; Kent et al., 1994; Dunn et al., 2000). More recent studies of Axial Seamount, a hotspot volcano centered on the intermediate-spreading Juan de Fuca Ridge (JdFR), revealed a complex upper-crustal magma reservoir with high inferred melt fractions over a deeper mush zone (West et al., 2003; Arnulf et al., 2014a, 2018). While much is known about the detailed geometry and properties of the shallow magma bodies in these submarine systems, most geophysical studies conducted to date can resolve only large-scale average properties in the lower crust (Dunn et al., 2000; West et al., 2003; Arnoux et al., 2019), and comparatively little is known about the distribution of melt or melt transport processes within the inferred mush zone. Important questions such as how melt is delivered from the mantle, how melt migrates through the lower crust to replenish the shallow reservoir, and what triggers dike intrusion and eruption events are poorly understood (e.g., Korenaga and Kelemen, 1998; Lissenberg et al., 2013; Sparks et al., 2019).

DATA

Here, we present new seismic reflection images from Axial Seamount that reveal a deep crustal feeder zone within the inferred mush beneath the broad shallow main magma reservoir (MMR; Arnulf et al., 2014a), which underlies the summit caldera of this submarine volcano (Fig. 1). Multi-channel seismic (MSC) were acquired in 2002 using a 6-km-long, 480 channel streamer with 12.5 m receiver intervals and a 49.16 L (3000 cubic inch) source array fired every 37.5 m (Carbotte et al., 2006). Reverse time-migration (RTM) was conducted following the procedure described in Arnulf et al. (2014a) on two previously studied perpendicular lines crossing the caldera (Figs. 1 and 2), with the migration extended to include deeper parts of the section to 6.5 km below sea level (bsl). In addition, poststack time-migrated sections that include the layer 2A event and that represent more minimally processed sections for the deeper crust were also generated for both lines, as well as a third line, which followed the modern eruption zone along the southeastern edge of the caldera (see Figs. S1 and S2 in the GSA Supplemental Materials[1]).

RESULTS AND DISCUSSION

The seismic images show the prominent reflection marking the top of the MMR located at 1.1–2.0 km below seafloor (bsf), as well as a weak subparallel bottom reflection, which is interpreted to be a 600-m-thick to >1-km-thick magma reservoir (Fig. 2; Fig. S2; Arnulf et al., 2014a). This reservoir, which underlies the full extent of the caldera, is geometrically complex, composed of a shallower, more melt-rich portion in the southeast and a deeper, more mushy body

CITATION: Carbotte, S.M., et al., 2020, Stacked sills forming a deep melt-mush feeder conduit beneath Axial Seamount: Geology, v. 48, p. , https://doi.org/10.1130/G47223.1

Downloaded from https://pubs.geoscienceworld.org/gsa/geology/article-pdf/4984067/g47223.pdf
by Columbia University user

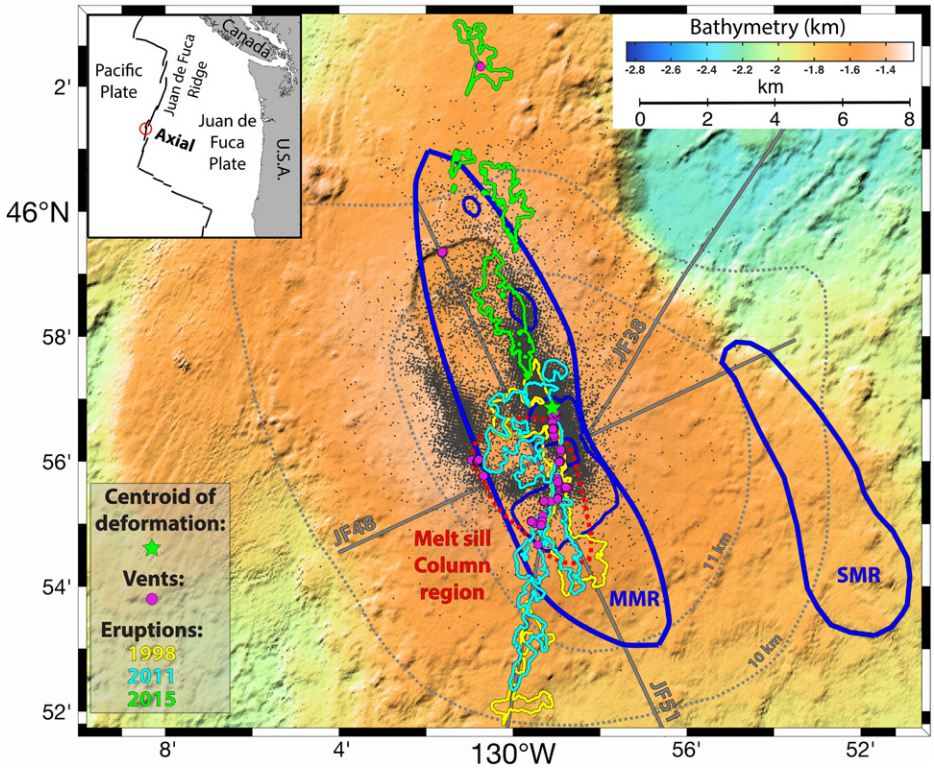

Figure 1. Bathymetric map of Axial Seamount showing location of lower-crust melt conduit and relationships with other magmatic features. Red line—inferred maximum plan-view extent of melt lens conduit; gray solid lines—locations of seismic sections (Fig. 2; Fig. S2 [see text footnote 1]); blue lines—extent of main and secondary magma reservoirs (MMR and SMR) identified in Arnulf et al. (2014a, 2018), with shallowest portion (2.9 km below sea level) in thinner line. Recent lava flows are color coded for eruption year as in legend (from Caress et al., 2012; Chadwick et al., 2013, 2016). Crustal thickness from West et al. (2003) is shown with gray dashed lines. Locations of hydrothermal vent fields are indicated with purple dots; green star marks centroid of pressure source from Nooner and Chadwick (2016); black dots show seismicity detected prior and during 2015 eruption (Arnulf et al., 2018).

[1]Supplemental Material. Discussion of potential artifacts to aid interpretation of seismic data; discussion of one-dimensional finite element model for multi-phase flow in a viscoelastic matrix including model parameters used; Figures S1–S6 including post stack time emigration images for lines 38, 48, and 51; partial offset stacks; pre-stack data examples; and velocity models used for reverse-time migration. Please visit https://doi.org/10.1130/GEOL.26213S.12101256 to access the supplemental material, and contact editing@geosociety.org with any questions. Data Sources: multichannel seismic data used in this study are available through the Marine Geoscience Data System (http://www.marine-geo.org/tools/search/entry.php?id=EW0207). Bathymetric data are from the GMRT Synthesis (http://www.marine-geo.org/tools/maps_grids.php). Hypocentral earthquake estimates for the 2015 Axial Seamount eruptive sequence and tomographic velocity models are archived with the Marine Geoscience Data System (Arnulf, Harding, Kent, and Wilcock, 2018, https://doi.org/10.1594/IEDA/324421, https://doi.org/10.1594/IEDA/324420). Interpretive outlines of the documented eruptions are available from Chadwick et al. (2014, https://doi.org/10.1594/IEDA/321222, https://doi.org/10.1594/IEDA/323601); Clague et al. (2018, https://doi.org/10.1594/IEDA/324416, https://doi.org/10.1594/IEDA/324418), and Clague et al. (2018, https://doi.org/10.1594/IEDA/324415, https://doi.org/10.1594/IEDA/324417).

in the northwest, as inferred from reflection amplitude characteristics and the presence/absence of converted shear arrivals (Arnulf et al., 2014a).

Beneath this shallow reservoir, the new images reveal a vertical conduit of deeper subhorizontal reflections that extends to depths of ~5 km bsf; this region is ~3 km wide by ~5 km long in map view, roughly centered beneath the southern shallowest portion of the upper-crustal reservoir (Figs. 1 and 2; Fig. S2). On each seismic line, ~4–6 bright reflections can be identified, spaced ~300–450 m apart, with the deepest event located ~2 km below the shallow MMR. The top of the shallow reservoir located above the deep column of reflections is characterized by high-reflection amplitudes consistent with high melt content.

Based on considerations of their geometry and seismic source-receiver offset characteristics, the possibility that the deep events could reflect artifacts such as internal multiples or out-of-plane scattering from the seafloor, or that they may be converted shear wave arrivals, is unlikely (see the Supplemental Materials and Figs. S3–S5). We conclude that these events are true reflections from structures in the crust, similar to those observed previously below the axial magma lens (AML) along the East Pacific Rise (EPR; Marjanović et al., 2014; Arnulf et al., 2014b). Given the low signal-to-noise ratio of the reflections, quantitative studies of the material properties of the source bodies cannot be conducted using the existing seismic data. However, from their location within the mid-to-lower crust where high melt fluxes are expected, and similarities with the events detected beneath the EPR, the most plausible explanation is that they arise from magma bodies. Furthermore, imaging a vertically stacked series of events deep into the crust requires limited signal attenuation both through the broad shallow MMR and within the event column. Previous studies of the AML reflector found beneath nearby portions of the JdFR indicated a thin (<100 m) reservoir of melt floored by a partially solid mush zone where velocities were 1–2 km/s higher than in the magma lens (Canales et al., 2006). The vertically stacked reflections beneath the shallow MMR are likely to be similar thin zones of melt within a higher-velocity mush matrix with limited melt content.

MELT LENS CONDUIT AND RECENT HISTORY OF ERUPTIONS AND CALDERA INFLATION

The three eruptions at Axial Seamount that are documented occurred in 1998, 4 yr prior to the reflection survey, and in 2011 and 2015, 9 and 13 yr after the survey, respectively. All three eruption/dike intrusion events initiated within the southeastern portion of the caldera (Chadwick et al., 2013, 2016; Caress et al., 2012; Wilcock et al., 2016). The primary lava flows that erupted during both the 1998 and 2011 events are focused within this region (Fig. 1), and many other characteristics of these two eruptions are remarkably similar, including the timing of geophysical precursory signals and the location of eruptive fissures (Chadwick et al., 2013). Seafloor eruptions from the 2015 event are located north of the 1998 and 2011 eruptions. However, tilt meter records and detected microseismicity spanning the eruption suggest the initial dike intrusion was sourced in part from the same region of the shallow melt reservoir as for the earlier eruptions (Nooner and Chadwick, 2016; Chadwick et al., 2016; Wilcock et al., 2016).

We interpret the stacked melt lenses as a deep crustal conduit that feeds the shallowest melt-rich portion of the upper-crustal magma reservoir, which is the inferred source region for the three historical eruptions (Figs. 1 and 2; Fig. S2). We conclude that magma flux within this pipe was linked to the initiation of all three eruptions and that focused melt delivery and corresponding higher heat flux from this deep conduit account for the local shoaling of the MMR to 1.1 km bsf above the center of the melt lens column. This deep conduit is also roughly centered within the

Downloaded from https://pubs.geoscienceworld.org/gsa/geology/article-pdf/4984067/g47223.pdf
by Columbia University user

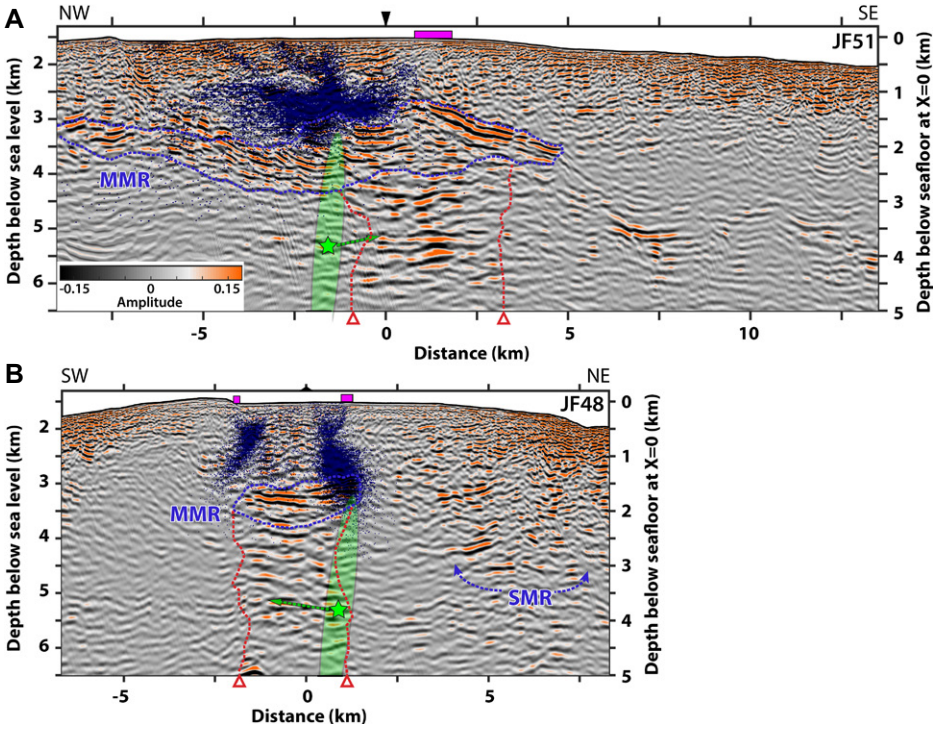

Figure 2. (A–B) Reverse time-migration images showing melt lens conduit beneath main magma reservoir (MMR) at Axial Seamount, along lines 51 (A) and 48 (B). Blue lines—interpreted top and bottom of MMR. Red lines—melt column region. Green shaded region—projected location of inflation source modeled from geodetic data (from Nooner and Chadwick, 2016), with green star marking centroid depth and arrow indicating projection of revised centroid from Hefner et al. (2019). Hydrothermal vents are shown in purple. Blue dots show hypocenters of all earthquakes from Figure 1 located (A) beneath east caldera wall and (B) within 5 km from seismic section (from Arnulf et al., 2018). Origin for distance scale is line 48–51 intersection. SMR—secondary magma reservoir.

region of thickest crust beneath Axial Seamount (up to 11 km; Fig. 1; West et al., 2003), consistent with the interpretation that this is a long-term magma conduit linked to the current location of the Cobb-Eickelberg hotspot (Wilcock et al., 2016; Arnulf et al., 2018).

Three decades of seafloor geodetic studies document a history of steady seamount inflation during intereruption periods and rapid deflation associated with the three eruptions (Nooner and Chadwick, 2016). From modeling of geodetic records prior to and during the 2015 event, Nooner and Chadwick (2016) obtained a best-fit pressure source that corresponds to a steeply dipping, prolate spheroid centered at 3.8 km bsf, with the top terminating at ~1.6 km bsf, at the depth of the shallow MMR (Figs. 1 and 2). It is important to note that the inflation/deflation records spanning this eruption period cannot be well fit with pressure changes in a subhorizontal body approximating the broad MMR, but, rather, a deeper, narrow, nearly vertical conduit is indicated.

The pressure source derived from geodetic modeling is remarkably similar in geometry and depth extent to the quasi-vertical conduit of stacked lenses imaged in our study. The model source is offset from and is narrower (2.2×0.4 km) than the melt column (Figs. 1 and 2). However, the geodetic source was derived assuming an inflating body embedded within a uniform elastic medium and is expected to provide a minimum estimate of the size of the inflation source, with significant uncertainties in location due to both data and model limitations. Indeed, recent geodetic modeling that subtracts the observed slip on the caldera-bounding faults locates the pressure source closer to the center of our conduit (Fig. 2; Hefner et al., 2019). We conclude that the deep melt lens column revealed in our images from 2002 is the inflation/deflation source for the recent eruptions, with the MCS data defining its location and revealing an internal structure composed of a series of melt lenses embedded within a more crystalline mush.

Further support for this interpretation comes from the abundant microseismicity detected prior to and during the 2015 eruption (Wilcock et al., 2016; Arnulf et al., 2018). Seismicity is largely confined to the shallow crust, above the MMR (Figs. 1 and 2), and for the pre-eruption period, it was concentrated on outward-facing ring faults along the south-central portion of both the east and, to lesser extent, west caldera walls, with normal fault mechanisms consistent with inflation of the underlying magma reservoir (Levy et al., 2018). Additionally, two diffuse bands of seismicity crossed the caldera floor, one of which coincided with the northern edge of the melt lens column. Whereas this subset of inflation-related seismicity is difficult to explain with the location of the Nooner and Chadwick (2016) geodetic model source, it is consistent with fracturing of the shallow crust linked to inflation centered within the imaged melt column.

ORIGIN OF MELT LENSES WITHIN A MUSH CONDUIT

What could give rise to the multiple, thin, horizontally aligned, melt-rich bodies within a deep conduit beneath the MMR? The long-term record of steady intereruption volcano inflation is attributed to magma recharge at depth and ascent of melt via porous flow within a conduit beneath the MMR (Nooner and Chadwick, 2009, 2016; Chadwick et al., 2012). Our observations of quasi-regularly spaced lenses in the region of the volcano inflation source are suggestive of porosity waves, which have been long predicted from analytic and numerical models of melt segregation from a mush via compaction in the mantle (e.g., McKenzie, 1984; Spiegelman, 1993a, 1993b; Rabinowicz et al., 2001) and more recently considered for silicic crustal systems (e.g., Jackson et al., 2018). Compaction refers to the coupled process of melt migration and matrix deformation whereby melt within a viscously deformable matrix ascends and can organize into localized excesses of melt that propagate through the matrix as waves driven by the relative buoyancy of melt and the surrounding crystalline matrix. Porosity waves will be generated from any obstruction in the melt flux (Spiegelman, 1993b) and, in the case of a stationary obstruction due to a freezing front or rheological barrier, can evolve into standing waves aligned with the barrier (Spiegelman, 1993a).

The thermally controlled permeability barrier that governs the depth of the MMR (Arnulf et al., 2018; Phipps Morgan and Chen, 1993) could provide the obstruction needed for the development of solitary porosity waves below. Results from a one-dimensional viscoelastic model using the approximate depth of the MMR and melt fractions of 20% for the shallow portions of the underlying mush zone (West et al., 2003; Arnulf et al., 2018), with plausible melt and mush viscosities and mush permeabilities for this mafic system (e.g., Fontaine et al., 2017; Sparks et al., 2019), predict a series of porosity waves with similar quasi-regular spacings occurring over a similar depth range as the observed melt lenses (Fig. 3; see also the Supplemental Material). While the specific spacing and amplitude of the waves will scale with the relative size of the flux obstruction and length of compaction, the production of these melt-rich segregations is a robust feature of fluid flow in viscously deformable media (Spiegelman, 1993a, 1993b).

The emerging consensus view of magmatic plumbing systems at volcanos is that sites of

Downloaded from https://pubs.geoscienceworld.org/gsa/geology/article-pdf/4984067/g47223.pdf
by Columbia University user

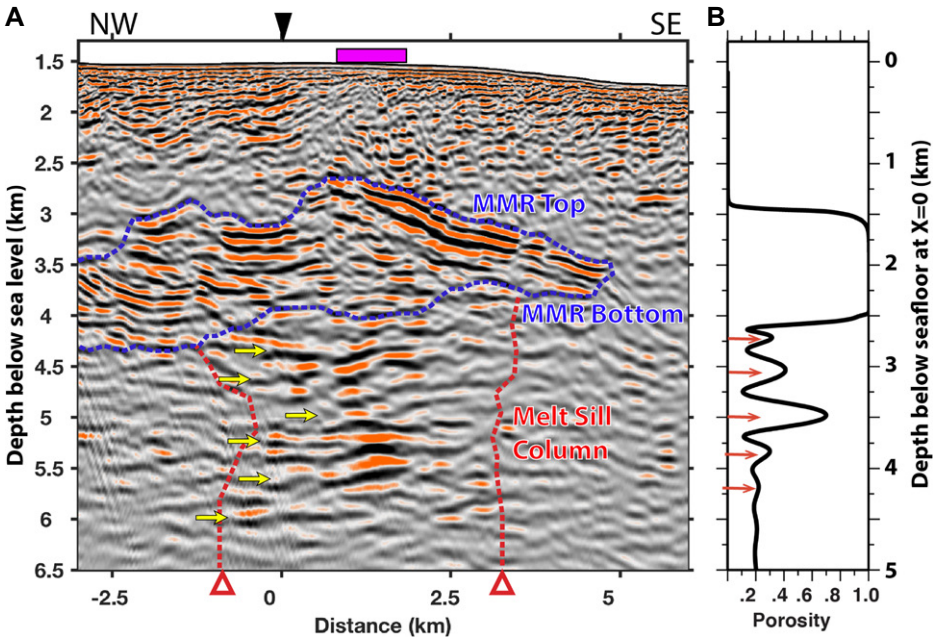

Figure 3. Comparison of observed melt conduit with numerical model of porosity waves. (A) Close-up of line 51 highlighting melt sill conduit. MMR—main magma reservoir. (B) Melt fraction as function of depth showing simulated regions of high melt fraction (porosity) calculated using one-dimensional finite element model for multiphase flow in viscoelastic matrix with an approximation for melt flow into freezing and strengthening upper lid (see supplemental material for further model details [text footnote 1]). Model uses melt fraction of 20%, melt viscosity of 2 Pa·s, and mush viscosity of 4×10^{16} Pa s and results in local zones of high melt fraction beneath simulated shallow magma reservoir with ~400 m spacing, similar to spacing of subhorizontal melt lenses imaged beneath Axial Seamount (~300–450 m) shown in A.

melt accumulation and storage likely form at multiple levels within a crystal mush–dominated reservoir (Cashman et al., 2017; Sparks et al., 2019). At active subaerial volcanos, observations of seismic anisotropy indicative of the presence of horizontally layered melt in the midcrust have been found (e.g., Jaxybulatov et al., 2014; Harmon and Rychert, 2015), and melt lenses within the midcrust mush zone have been detected beneath mid-ocean ridges (Marjanović et al., 2014; Arnulf et al., 2014b). Multiple processes of intrusion, remobilization, and mush compaction may contribute to the formation of melt accumulations within magmatic systems (Sparks et al., 2019), and detailed images of the architecture of these zones are needed to understand their origin. The observations from Axial Seamount presented here, which reveal the presence of near-regular-spaced melt segregations within a mush feeder conduit beneath a shallow magma reservoir, are unique for any active volcano and indicate possible formation via mush compaction. Recently acquired three-dimensional MCS data from Axial Seamount (Arnulf et al., 2019) will provide much higher-resolution images of the melt conduit and further constraints on the zonation and physical state of melt within the volcanic edifice.

ACKNOWLEDGMENTS

We thank Terry Plank and Peter Kelemen for helpful discussions and William Chadwick, Richard Hobbs, and William Wilcock for thorough reviews, which improved the manuscript. Data processing was conducted in part with Landmark© software. Data collection and processing were supported by National Science Foundation grants OCE0002488 (Lamont-Doherty Earth Observatory); 0002551 (Woods Hole Oceanographic Institution); 0002600, 1357076, and 1658018 (Scripps Institution of Oceanography); and 1658199 (University of Texas Institute for Geophysics); and Columbia University.

REFERENCES CITED

Annen, C., Blundy, J.D., and Sparks, R.S.J., 2005, The genesis of intermediate and silicic magmas in deep crustal hot zones: Journal of Petrology, v. 47, p. 505–539, https://doi.org/10.1093/petrology/egi084.

Arnoux, G.M., Toomey, D.R., Hooft, E.E.E., and Wilcock, W.S.D., 2019, Seismic imaging and physical properties of the Endeavour segment: Evidence that skew between mantle and crustal magmatic systems governs spreading center processes: Geochemistry Geophysics Geosystems, v. 20, p. 1319–1339, https://doi.org/10.1029/2018GC007978.

Arnulf, A.F., Harding, A.J., Kent, G.M., Carbotte, S.M., Canales, J.P., and Nedimović, M.R., 2014a, Anatomy of an active submarine volcano: Geology, v. 42, p. 655–658, https://doi.org/10.1130/G35629.1.

Arnulf, A.F., Singh, S.C., and Pye, J.W., 2014b, Seismic evidence of a complex multi-lens melt reservoir beneath the 9°N overlapping spreading center at the East Pacific Rise: Geophysical Research Letters, v. 41, p. 6109–6115, https://doi.org/10.1002/2014GL060859.

Arnulf, A.F., Harding, A.J., Kent, G.M., and Wilcock, W.S.D., 2018, Structure, seismicity, and accretionary processes at the hot spot–influenced Axial Seamount on the Juan de Fuca Ridge: Journal of Geophysical Research, v. 123, p. 4618–4646, https://doi.org/10.1029/2017JB015131.

Arnulf, A.F., Harding, A.J., Saustrup, S., Kell, A.M., Kent, G.M., Carbotte, S.M., Canales, J.-P., Nedimovic, M.R., Bellucci, M., Brandt, S., Cap, A., Eischen, T.E., Goulain, M., Griffiths, M., Lee, M., Lucas, V., Mitchell, S.J., and Oller, B., 2019, Imaging the internal workings of Axial Seamount on the Juan de Fuca Ridge: San Francisco, California, American Geophysical Union Fall Meeting, abstract OS51B–148.

Canales, J.P., Singh, S.C., Detrick, R.S., Carbotte, S.M., Harding, A., Kent, G.M., Diebold, J., Babcock, J., and Nedimović, M.R., 2006, Seismic evidence for variations in axial magma chamber properties along the southern Juan de Fuca Ridge: Earth and Planetary Science Letters, v. 246, p. 353–366, https://doi.org/10.1016/j.epsl.2006.04.032.

Carbotte, S.M., Detrick, R.S., Harding, A., Canales, J.P., Babcock, J., Kent, G., Van Ark, E., Nedimovic, M., and Diebold, J., 2006, Rift topography linked to magmatism at the intermediate spreading Juan de Fuca Ridge: Geology, v. 34, p. 209–212, https://doi.org/10.1130/G21969.1.

Caress, D.W., Clague, D.A., Paduan, J.B., Martin, J.F., Dreyer, B.M., Chadwick, W.W., Jr., Denny, A., and Kelley, D.S., 2012, Repeat bathymetric surveys at 1-metre resolution of lava flows erupted at Axial Seamount in April 2011: Nature Geoscience, v. 5, p. 483–488, https://doi.org/10.1038/ngeo1496.

Cashman, K.V., Sparks, R.S.J., and Blundy, J.D., 2017, Vertically extensive and unstable magmatic systems: A unified view of igneous processes: Science, v. 355, p. 6331, https://doi.org/10.1126/science.aag3055.

Chadwick, W.W., Jr., Nooner, S.L., Butterfield, D.A., and Lilley, M.D., 2012, Seafloor deformation and forecasts of the April 2011 eruption at Axial Seamount: Nature Geoscience, v. 5, p. 474–477, https://doi.org/10.1038/ngeo1464.

Chadwick, W.W., Clague, D.A., Embley, R.W., Perfit, M.R., Butterfield, D.A., Caress, D.W., Paduan, J.B., Martin, J.F., Sasnett, P., Merle, S.G., and Bobbitt, A.M., 2013, The 1998 eruption of Axial Seamount: New insights on submarine lava flow emplacement from high-resolution mapping: Geochemistry Geophysics Geosystems, v. 14, p. 3939–3968, https://doi.org/10.1002/ggge.20202.

Chadwick, W.W., Paduan, J.B., Clague, D.A., Dreyer, B.M., Merle, S.G., Bobbitt, A.M., Caress, D.W., Philip, B.T., Kelley, D.S., and Nooner, S.L., 2016, Voluminous eruption from a zoned magma body after an increase in supply rate at Axial Seamount: Geophysical Research Letters, v. 43, p. 12–063, https://doi.org/10.1002/2016GL071327.

Dunn, R.A., Toomey, D.R., and Solomon, S.C., 2000, Three-dimensional seismic structure and physical properties of the crust and shallow mantle beneath the East Pacific Rise at 9°30′N: Journal of Geophysical Research, v. 105, p. 23537–23555, https://doi.org/10.1029/2000JB900210.

Fontaine, F.J., Rabinowicz, M., and Cannat, M., 2017, Can high-temperature, high-heat flux hydrothermal vent fields be explained by thermal convection in the lower crust along fast-spreading mid-ocean ridges?: Geochemistry Geophysics Geosystems, v. 18, p. 1907–1925, https://doi.org/10.1002/2016GC006737.

Downloaded from https://pubs.geoscienceworld.org/gsa/geology/article-pdf/4984067/g47223.pdf
by Columbia University user

Harmon, N., and Rychert, C.A., 2015, Seismic imaging of deep crustal melt sills beneath Costa Rica suggests a method for the formation of the Archean continental crust: Earth and Planetary Science Letters, v. 430, p. 140–148, https://doi.org/10.1016/j.epsl.2015.07.062.

Hefner, W., Nooner S.L., Chadwick, W.W., Jr., Caress, D.W., Bohnenstiehl, D., Paduan, J.B., and Clague, D.A., 2019, Magmatic deformation models including caldera-ring faulting for the 2015 eruption of Axial Seamount: San Francisco, California, American Geophysical Union Fall Meeting, abstract OS51B–1486.

Jackson, M.D., Blundy, J., and Sparks, R.S.J., 2018, Chemical differentiation, cold storage and remobilization of magma in the Earth's crust: Nature, v. 564, p. 405–409, https://doi.org/10.1038/s41586-018-0746-2.

Jaxybulatov, K., Shapiro, N.M., Koulakov, I., Mordret, A., Landes, M., and Sens-Schonfelder, C., 2014, A large magmatic sill complex beneath the Toba caldera: Science, v. 346, p. 617–619, https://doi.org/10.1126/science.1258582.

Kent, G.M., Harding, A.J., Orcutt, J.A., Detrick, R.S., Mutter, J.C., and Buhl, P., 1994, Uniform accretion of oceanic crust south of the Garrett transform at 14°15′S on the East Pacific Rise: Journal of Geophysical Research, v. 99, p. 9097–9116, https://doi.org/10.1029/93JB02872.

Korenaga, J., and Kelemen, P.B., 1998, Melt migration through the oceanic lower crust: A constraint from melt percolation modeling with finite solid diffusion: Earth and Planetary Science Letters, v. 156, p. 1–11, https://doi.org/10.1016/S0012-821X(98)00004-1.

Levy, S., Bohnenstiehl, D.R., Sprinkle, P., Boettcher, M.S., Wilcock, W.S.D., Tolstoy, M., and Waldhauser, F., 2018, The mechanics of fault re-activation surrounding the 2015 eruption of Axial Seamount: Geology, v. 46, p. 447–450, https://doi.org/10.1130/G39978.1.

Lissenberg, C.J., MacLeod, C.J., Howard, K.A., and Godard, M., 2013, Pervasive reactive melt migration through fast-spreading lower oceanic crust (Hess Deep, equatorial Pacific Ocean): Earth and Planetary Science Letters, v. 361, p. 436–447, https://doi.org/10.1016/j.epsl.2012.11.012.

Marjanović, M., Carbotte, S.M., Carton, H., Nedimović, M.R., Mutter, J.C., and Canales, J.P., 2014, A multi-sill magma plumbing system beneath the axis of the East Pacific Rise: Nature Geoscience, v. 7, p. 825–829, https://doi.org/10.1038/ngeo2272.

McKenzie, D.A.N., 1984, The generation and compaction of partially molten rock: Journal of Petrology, v. 25, p. 713–765, https://doi.org/10.1093/petrology/25.3.713.

Nooner, S.L., and Chadwick, W.W., 2009, Volcanic inflation measured in the caldera of Axial Seamount: Implications for magma supply and future eruptions: Geochemistry Geophysics Geosystems, v. 10, Q02002, https://doi.org/10.1029/2008GC002315.

Nooner, S.L., and Chadwick, W.W., 2016, Inflation-predictable behavior and co-eruption deformation at Axial Seamount: Science, v. 354, p. 1399–1403, https://doi.org/10.1126/science.aah4666.

Phipps Morgan, J., and Chen, Y.J., 1993, The genesis of oceanic crust: Magma injection, hydrothermal circulation, and crustal flow: Journal of Geophysical Research, v. 98, p. 6283–6297, https://doi.org/10.1029/92JB02650.

Rabinowicz, M., Genthon, P., Ceuleneer, G., and Hillairet, M., 2001, Compaction in a mantle mush with high melt concentrations and the generation of magma chambers: Earth and Planetary Science Letters, v. 188, p. 313–328, https://doi.org/10.1016/S0012-821X(01)00330-2.

Sinton, J.M., and Detrick, R.S., 1992, Mid-ocean ridge magma chambers: Journal of Geophysical Research, v. 97, p. 197–216, https://doi.org/10.1029/91JB02508.

Sparks, R.S.J., Annen, C., Blundy, J.D., Cashman, K.V., Rust, A.C., and Jackson, M.D., 2019, Formation and dynamics of magma reservoirs: Philosophical Transactions of the Royal Society of London, ser. A, Mathematical and Physical Sciences, v. 377, p. 20180019, https://doi.org/10.1098/rsta.2018.0019.

Spiegelman, M., 1993a, Physics of melt extraction: Theory, implications and applications: Philosophical Transactions of the Royal Society of London: Ser. A, Mathematical and Physical Sciences, v. 342, p. 23–41.

Spiegelman, M., 1993b, Flow in deformable porous media. Part 1: Simple analysis; Part 2: Numerical analysis—The relationship between shock waves and solitary waves: Journal of Fluid Mechanics, v. 247, p. 17–38, https://doi.org/10.1017/S0022112093000369.

West, M., Menke, W., and Tolstoy, M., 2003, Focused magma supply at the intersection of the Cobb hotspot and the Juan de Fuca Ridge: Geophysical Research Letters, v. 30, p. 1724, https://doi.org/10.1029/2003GL017104.

Wilcock, W.S., Tolstoy, M., Waldhauser, F., Garcia, C., Tan, Y.J., Bohnenstiehl, D.R., Caplan-Auerbach, J., Dziak, R.P., Arnulf, A.F., and Mann, M.E., 2016, Seismic constraints on caldera dynamics from the 2015 Axial Seamount eruption: Science, v. 354, p. 1395–1399, https://doi.org/10.1126/science.aah5563.

Printed in USA

Downloaded from https://pubs.geoscienceworld.org/gsa/geology/article-pdf/4984067/g47223.pdf
by Columbia University user